Asian Journal of Pharmaceutical Sciences 16 (2021) 762–771

Available online at www.sciencedirect.com

ScienceDirect

journal homepage: www.elsevier.com/locate/AJPS

Original Research Paper

Carrier-free prodrug nanoparticles based on dasatinib and cisplatin for efficient antitumor *in vivo*

Lu Yang, Jiaxi Xu, Zheng Xie, Faquan Song, Xin Wang, Rupei Tang**

Engineering Research Center for Biomedical Materials, Anhui Key Laboratory of Modern Bio-manufacturing, School of Life Science, Anhui University, Hefei 230601, China

ARTICLE INFO

Article history:
Received 6 May 2021
Revised 19 July 2021
Accepted 4 August 2021
Available online 8 September 2021

Keywords:
Prodrug
Nanoparticle
Dasatinib
Cisplatin

ABSTRACT

Carrier-free drug self-delivery systems consisting of amphiphilic drug-drug conjugate (ADDC) with well-defined structure and nanoscale features have drawn much attention in tumor drug delivery. Herein, we report a simple and effective strategy to prepare ADDC using derivatives of cisplatin (CP) and dasatinib (DAS), which further self-assembled to form reduction-responsive nanoparticles (CP-DDA NPs). DAS was modified with succinic anhydride and then connected with CP derivative by ester bonds. The size, micromorphology and *in vitro* drug release of CP-DDA NPs were characterized. The biocompatibility and bioactivity of these carrier-free nanoparticles were then investigated by HepG2 cells and H22-tumor bearing mice. *In vitro* and *in vivo* experiments proved that CP-DDA NPs had excellent anti-tumor activity and significantly reduced toxicities. This study provides a new strategy to design the carrier-free nanomedicine composed of CP and DAS for synergistic tumor treatment.

1. Introduction

Chemotherapy suffers from some limitations such as poor solubility, low bioavailability, rapid blood clearance, random distribution, insufficient tumor accumulation, severe side effects on normal organs, and the development of multidrug resistance (MDR) during treatment [1–3]. Carrier-assistant anticancer drug delivery systems (DDSs) are a promising therapeutic strategy to achieve a better therapeutic efficacy and lower side-effects compared with free drugs [4–7]. Commonly, chemotherapeutics are encapsulated in various nanocarriers such as nanoparticles, liposomes and vesicles, and the unique size and surface characteristics lead to the passive accumulation at tumor areas via enhanced permeability and retention (EPR) effect [8–10]. However, most carrier materials have no substantial curative effect on tumors and these excipients can generate unexpected toxicity and immune response during degradation, metabolism and excretion in the body [11–13]. In addition, the process of designing and synthesizing the carrier is relatively complicated, which further leads to batch-to-batch variation in the drug metabolism process and drug therapeutic effects of carrier-based nanomedicine [14–17].

* Corresponding author.
E-mail addresses: wx2832@163.com (X. Wang), tangrp99@iccas.ac.cn (R.P. Tang).
Peer review under responsibility of Shenyang Pharmaceutical University.

https://doi.org/10.1016/j.ajps.2021.08.001

Aiming at these problems, a lot of research has been done to develop carrier-free drug self-delivery systems based on amphiphilic drug-drug conjugate (ADDC) [18–20]. ADDC is an amphiphilic molecule formed by connecting hydrophilic drugs and hydrophobic drugs through chemical bonds, which can self-assemble into nano-drugs by hydrophobic forces to realize drug self-delivery [21, 22]. These carrier-free DDSs possess well-defined structures, precise drug ratios, high drug loading capacity and low-toxicity metabolic pathways [3,23,24]. Various stimulus-reactive chemical bonds such as ester bonds, hydrazone bonds, disulfide bonds, have been used to construct ADDC to control the drug releasing behavior. In addition, multiple drugs or fluorescent agents can be simultaneously loaded into these DDSs to provide a synergistic antitumor effect or to guide chemotherapy.

Yan et al. reported an ADDC based on irinotecan (Ir) and chlorambucil (Cb) linked by ester bond. The conjugate self-assembled DDSs exhibited higher stability and improved blood circulation. After cellular uptake, the ester bonds in ADDC were hydrolyzed and Ir and Cb were released, exerting outstanding antitumor activity [25]. Hou et al. developed an ADDC nanoparticle (MTX-SS-PPT NAs) based on methotrexate (MTX) and podophyllotoxin (PPT), whose disulfide bond in the structure facilitates the degradation of MTX-SS-PPT NAs under reductive conditions in tumor cells to accurately release the active drug. In addition, MTX was able to target folic acid overexpressing tumor cells. The results indicated that the nano-formulation could significantly enhance the biocompatibility and decrease the toxicity of PPT [22]. Thus, it should be simple, effective and promising strategy to construct the carrier-free DDSs based on ADDC for synergistic cancer therapy.

Src, a non-receptor tyrosine protein kinase, plays a crucial role in many cellular signaling pathways [26,27]. It was reported that Src liveness and levels are prominently elevated in various tumors, and involved in tumor cell proliferation, migration, and angiogenesis, thereby promoting tumor growth [28–30]. Dasatinib (DAS) is an ATP-based competitive orally active dual Src/Abl kinase inhibitor, which can inhibit a variety of Src signaling pathways and further inhibit tumor cell migration, invasion and angiogenesis [27,31]. DAS also showed antitumor activity in some solid tumors [32,33]. In addition, various studies demonstrated that the combination of DAS and other chemotherapeutics could realize synergistic antitumor effect. Li reported two novel prodrug polymers consisted of poly(oligo(ethylene glycol) methacrylate) (POEG) hydrophilic blocks and DAS-conjugated hydrophobic blocks, which were designed as dual-functional carriers for codelivery with doxorubicin (DOX). The system facilitated efficient cleavage of DAS and DOX from prodrug micelles in tumor cells/tissues, leading to a higher level of anti-tumor activity *in vitro* and *in vivo*. This redox-responsive prodrug micellar system provides an attractive strategy for effective combination of DOX and DAS [34]. In another study, the authors demonstrated that DAS could enhance paclitaxel (PTX) and gemcitabine (GEM) inhibitory activity in human pancreatic cancer cells. DAS could enhance the efficacy of PTX or GEM by reducing the cell viability and inhibiting the cell proliferation. DAS with PTX or GEM combination exhibited higher inhibition of the cell migration ability than single agent alone. The combination of DAS with PTX or GEM also inhibited p-SRC, p-STAT3, p-AKT, and/or p-ERK in these pancreatic cancer cells. Therefore, the results demonstrated that combined DAS and PTX or GEM therapy could be a viable therapeutic approach for human pancreatic cancer [35]. Zhan reported that DAS could enhance cisplatin (CP) sensitivity in human esophageal squamous cell carcinoma (ESCC) cells via suppression of PI3K/AKT and Stat3 pathways [36]. CP Pt(II)) can cross-link the DNA double strand, thereby inhibiting DNA replication and inducing apoptosis in tumor cells. Diamminedichlorodihydroxyplatinum (DH–CP) is an octahedrally coordinated derivative of cisplatin, and two hydroxyl groups on the DH–CP center provide more possibilities for further functionalization. Furthermore, Pt(IV) can be reduced to Pt(II) by glutathione (GSH) overexpressed in tumor cells to regain their antitumor ability [37–39]. Therefore, the carrier-free delivery system of small molecule NDDS based on Pt(IV) and DAS is expected to achieve a good synergistic anti-tumor effect.

Herein, we reported a novel carrier-free drug self-delivery system on the account of the ADDC strategy. First, the hydrophobic drug DAS was modified with succinic anhydride, and then connected with the hydrophilic DH–CP through ester bonds to obtain an amphiphilic drug-drug conjugate, in which the ratio of DAS to DH–CP is 2:1 (denoted as CP-DDA). Due to its appropriate amphiphilicity, CP-DDA could self-assemble into stable nanoparticles in aqueous solution (denoted as CP-DDA NPs). Without using any excipients, CP-DDA NPs have appropriate stability during the circulation, and may increase the accumulation of drugs at the tumor site through the EPR effect. After cell uptake, cisplatin and DAS are released, which is attributed to the hydrolysis of the ester bond and the reduction of Pt(IV) to Pt(II) by GSH. DAS inhibits Src activity, down-regulates related pathway signals and suppress tumor proliferation, while CP interacts with DNA to induce cell apoptosis, and ultimately produce a synergistic anti-tumor effect [36,40,41].

2. Materials and methods

2.1. *Materials*

N, N-Dimethylformamide (DMF) was dried overnight with calcium hydride (98%, Aladdin), then distilled to use. Dasatinib (DAS) (99%) and O-(1H-benzotriazol-1-yl)-N,N,N',N'-tetramethyluronium tetrafluorob-orate (TBTU) (98%) and sodium diethyldithiocarbamate (98%) were obtained from Aladdin (Shanghai, China). Cisplatin (CP) was obtained from Shandong platinum source chemical Co. Ltd (Jinan, China). Anhydrous ethanol, hydrogen peroxide (30%), anhydrous ether, DMF, triethylamine (TEA), succinic anhydridedichloromethane (DCM), anhydrous methanol and pyridine were all purchased from Sinopharm Chemical Reagent Co., Ltd (Shanghai, China). Cell culture medium, trypsin and fetal bovine serum were bought from KeyGEN BioTECH (Nanjing, China). Poly(2-hydroxyethyl methacrylate) (PHEMA) and 3-(4, 5-dimethylthiazol-2-yl)−2, 5-diphenyl tetrazolium bromide (MTT) were bought from Sigma-Aldrich.

Male ICR mice (SPF, 18–22 g) were obtained from Animal Center of Anhui Medical University (Hefei, China).

2.2. Synthesis of DH-CP and DAC

As shown in Sheam 1A, CP was oxidized by H_2O_2 and lyophilized to obtain the product DH–CP (*cis*,*cis*,trans-[Pt(IV)-$(NH_3)_2Cl_2(OH)_2$]). The structure of DH–CP was detected by Fourier infrared spectroscopy (FTIR). The synthesis of DAC (N-(2–chloro-6- methyl phenyl)−2-[[6-[4-(2-carboxyethyl)-base] piperazine-1–2-methyl pyridine-4-base] amino]−1,3-thiazole-5- form-amide) is based on the previously reported method with slight modifications [42]. DAS (1 equiv) was dissolved in DMF (10 ml), add triethylamine (TEA) (2 equiv) and succinic anhydride (1 equiv), and reacted at 30 ± 0.2 °C for 72 h. DMF was removed and the resulting mixture was washed with CH_2Cl_2 and MeOH, and dried under vacuum to obtain white powder product DAC. The structure of DAC was detected by nuclear magnetic resonance (^{1}H NMR) and FTIR.

2.3. Synthesis of CP-DDA

DAC (2.5 equiv) and TBTU (3 equiv) were dissolved in 10 ml DMF, activated at room temperature for 2 h. TEA and DH–CP (1 equiv) were added and then the reaction was continued until DH–CP was completely dissolved and the solution turned bright yellow. The structure of CP-DDA was detected by ^{1}H NMR, Liquid Chromatograph Mass Spectrometer (LC-MS) and FTIR.

2.4. Preparation of CP-DDA NPs

The prepared CP-DDA was dissolved with pyridine and slowly dripped into the vortex deionized water. Pyridine was removed by dialysis and then freeze-dried to obtain CP-DDA NPs. The diameter of CP-DDA NPs were measured by dynamic light scattering (DLS) in PB solution (pH 7.4) and cell culture medium with 10% FBS. A drop of CP-DDA solution (0.5 mg/ml) was added on the surface of a silicon wafer and dried at room temperature overnight. The micromorphology of CP-DDA NPs was detected by scanning electron microscope (SEM, REGULUS 8230).

2.5. In vitro drug release of DAS and CP

The drug release behavior of CP-DDA NPs was studied under four different conditions: pH7.4, pH7.4 with 2 uM GSH, pH6.0 and pH 6.0 with 10 mM GSH. Briefly, 0.5 ml of CP-DDA NPs (800 ug) was dialyzed with 10 ml PBS (pH 7.4 or the other conditions mentioned above) in a dialysis bag (MWCO 1000 Da) at 37 ± 0.2 °C. PBS contains 10% ethanol to promote the dissolution of DAS. Dialysate (10 ml) was collected and replenished with 10 ml of fresh buffer at predetermined time. The amounts of DAS released from CP-DDA NPs were measured using SpectraMax M2/M2e Microplate Readers (Molecular Devices, USA) at 320 nm. The amounts of CP released from CP-DDA NPs were measured using high performance liquid chromatography (HPLC, Thermo Scientific UltiMate 3000) with a diode-array detector and a C_{18} column (15 cm × 0.46 cm, Syncronis). 1 ml the release solution was taken, 200 ul of DDTC solution (5%) was added, vortex for 1 min, and then incubate in a 37 °C water bath for 30 min. 1 ml of chloroform was added for extraction, vortexed and mixed for 1 min, and centrifuged at 10 000 rpm for 10 min. Next, the lower layer of chloroform was aspirated and filtered. Detection wavelength was 254 nm; mobile phase: methanol: water (75:25, v/v); flow rate 1 ml/min; column temperature: 25 °C; injection volume: 10 ul.

2.6. In vitro cytotoxicity

H22 and HepG2 cells were seeded in 96-well plates at a density of 5×10^3 cells/well, and cultured for 24 h to allow the cells adherent. DAS, CP, DAS+CP and CP-DDA NPs with different drug concentrations were added and co-incubated for 24 h. Then, the medium was replaced with fresh medium containing 20 ul MTT solutions, incubated for 4 h, and 150 ul DMSO was added to each well and gently shaken to dissolve formazan. The absorbance of each well was detected at 570 nm with a microplate reader, and the cell survival rate was calculated.

2.7. Cell apoptosis measurement

H22 and HepG2 cells were seeded in 6-well plates at a density of 5×10^4 cells/well, and incubated for 24 h to allow the cells adherent. DAS (47.78 ug/ml), CP (16 ug/ml), DAS+CP (47.78l +16 ug/ml) and CP-DDA NPs (78.61 ug/ml) were added and co-cultured for 24 h. Cells were collected and apoptosis was detected by flow cytometry (BD FACSCalibur) stained with an Annexin V-FITC/PI Apoptosis Detection Kit (BestBio, China).

2.8. Evaluation of the healing and migration abilities of tumor cells In vitro

The HepG2 cell culture method was the same as Part 2.7. Before the addition of each drug, the pipet-gun was used to draw vertical lines in the culture hole, and drug concentration was quantified with CP (4 ug/ml). After 4 h, the drug-containing medium was replaced with fresh medium, and the scratch width was photographed and measured at 0, 24 and 48 h to calculate the healing rate. The calculation formula is as follows: $H = (A_t\text{-}A_0)/A_0$, where *A* represents the width of the scratch.

The HepG2 cell culture in the migration experiment was the same as above. After 4 h of co-incubation with each drug group, the cells were collected, suspended in 200 ul cell culture medium without serum and inoculated into the Transwell upper compartment. 1 ml cell culture medium was added to the lower compartment for further culture. After 48 h, the medium was discarded, the chambers were wiped with cotton swabs, and after fixed and stained of cells, observed under an inverted microscope, and photographed for statistics.

2.9. Preparation and growth inhibition study of HepG2 multi-cellular spheroids

Three-dimensional cultured multicellular spheroids (MCS) were established as previous reported works [39]. HepG2 cells were cultured in culture flasks whose bottom was covered

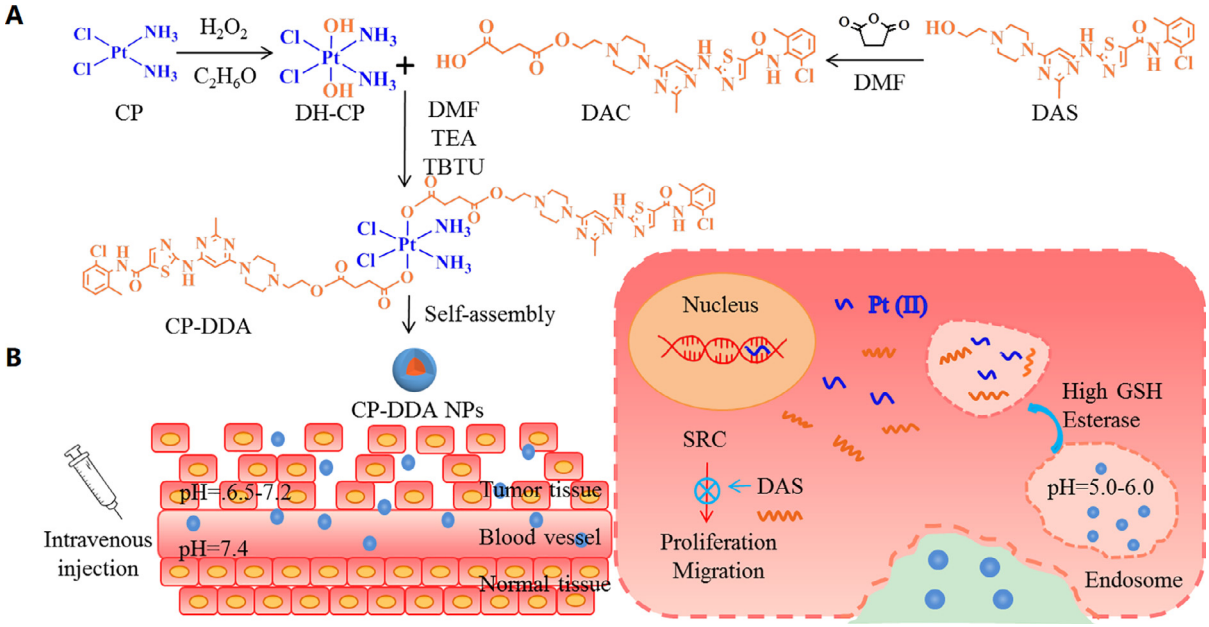

Scheme 1 – The synthetic route of CP-DDA NPs (A); Drug delivery mechanism of nanoparticles and drug release mechanism in tumor cells (B).

with PHEMA. During the culture process, the non-spherical and oversized MCS were removed and uniformly sized MCS continued to be cultured to about 150 um, and then, seeded in 96-well plates with the bottom covered with PHEMA. HepG2 MCS were co-cultured with DAS (47.78 ug/ml), CP (16 ug/ml), DAS+CP (47.78 + 16 ug/ml) and CP-DDA NPs (78.61 ug/ml), and the size and morphological changes of MCS were observed and recorded under the microscope.

2.10. *In vivo antitumor experiment and immunohistochemistry*

In vivo studies were followed by the protocols approved by the Institutional Animal Care and Use Committee, Anhui University, Ethical approval Number: IACUC, AHU Issue No. 2020–017. When the tumor volume of H22 increased to 50–100 mm^3, mice were randomly divided into 5 ($n = 11$) groups, and administrated with DAS, CP, DAS+CP and CP-DDA NPs via tail vein on Day 0 and Day 5, respectively. CP dose quantification was 4 mg/kg. Body weight and survival rate of mice were recorded. The tumor size was measured by vernier calipers every other day and its volume (V) was calculated according to the formula of $(a \times b^2)/2$, where a was the major axis and b was the minor axis [43]. During the treatment, one mouse was randomly selected from each group and the main organs and tumor were collected, stained using hematoxylin and eosin (H&E). The tissue damage was observed under a microscope and photographed.

2.11. *Statistical analysis*

All data were examined repeatedly three times and displayed as mean ± standard deviation (SD). Meanwhile all data were analyzed for statistical significance using Student's text, and P values less than 0.05 were considered statistically significant.

3. Results and discussion

3.1. *Characterization of DH-CP*

DH–CP, a Pt (IV) prodrug with reduction sensitivity was synthesized by oxidizing CP with H_2O_2, as shown in Scheme 1A. FTIR spectra of CP and DH–CP are shown in Fig. S1. Compared with CP (a), DH–CP (b) showed a narrow peak (1441.88 cm^{-1}) and sharp peak (3464.46 cm^{-1}) of -OH, which proved the correct structure of DH–CP.

3.2. *Characterization of DAC*

DAC was synthesized by the reaction of DAS with succinic anhydride (SA), as shown in Scheme 1A. ^1H NMR results of DAC (Fig. S2) were in line with the previously reported literature [37]. As for FTIR spectra (Fig. S1d), DAC showed absorption peaks of -C=O (1738.841 cm^{-1}) and -OC=O (1193.25 cm^{-1}). These results confirmed the successful preparation of DAC.

3.3. *Characterization of CP-DDA*

Based on the esterification of one molecule of DH–CP and two molecules of DAC, an ADDC was prepared, which is abbreviated as CP-DDA. The chemical structure of CP-DDA was confirmed by ^1H NMR, LC-MS and FT-IR. ^1H NMR spectrum of CP-DDA was presented in Fig. S3, compared with DAC (Fig. S2), a new peak of -NH_3 (peak n, 6.2–6.8 ppm) confirmed the formation of CP-DDA. The theoretical relative molecular weight of CP-DDA is 1475.28 (m/z, $[M+H]^+$), which is consistent with the MS measurement result (1475.3018, Fig. S4), and proves that the ratio of DAC to DH–CP in CP-DDA is 1:2. In addition the FTIR results (Fig. S1e) showed that the peak of DH–CP at 3459.42 cm^{-1} (-OH) disappeared after the reaction,

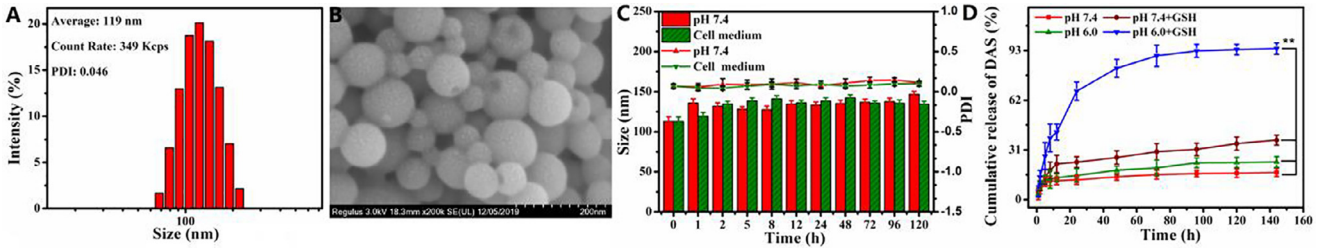

Fig. 1 – Characterization of CP-DDA NPs: Size and distribution (A); SEM images (B); the physiological stability: size and PDI change with PBS (pH 7.4) or cell culture medium (containing 10% FBS) (C); *In vitro* drug release of DAS (D).

and the peak of -C=O (1738.841 cm^{-1}) and -OC=O (1193.25 cm^{-1}) shift to 1723.97 cm^{-1} and 1191.40 cm^{-1}, which further proved that DH–CP and DAC combined through esterification reaction to produce CP-DDA. All results confirmed that CP-DDA had been synthesized successfully.

3.4. *Characterization of CP-DDA NPs*

A carrier-free ADDC self-delivery system was then prepared by self-assembly of CP-DDA in water, which was denoted as CP-DDA NPs. The hydrodynamic diameter and morphology of CP-DDA NPs were characterized by DLS and SEM. From Fig. 1A, the average size of CP-DDA NPs was 119 nm with a PDI of 0.046. SEM (Fig. 1B) also showed that CP-DDA NPs had a spherical structure with a mean size of 100 nm, which was consistent with that of DLS measurements. To investigate the physiological stability of the prepared nanoparticles, CP-DDA NPs were dispersed in PBS (pH 7.4) or cell culture medium (containing 10% FBS) for 120 h, respectively. The size and PDI change of CP-DDA NPs were detected by DLS (Fig. 1C). Obviously, there was no significant change during this period, indicating that CP-DDA NPs possessed excellent stability, which was beneficial to the drug delivery *in vivo* and enrichment to the tumor region through EPR effect [44].

3.5. *In vitro drug release of DAS and CP*

To further study the reduction triggered dissociation of the CD-DDA NPs, *in vitro* drug release was measured under four different conditions: pH 7.4; pH 7.4 with 2 uM GSH; pH 6.0 and pH 6.0 with 10 mM GSH. Fig. S5 displayed that the maximum UV absorption of DAS is 320 nm. The DAS release amount from CP-DDA NPs under different conditions were then measured at 320 nm, as shown in Fig. 1D. Under the condition of pH 6.0 with GSH (10 mM), the release of DAS reached 67.72% in 24 h and increased to 81.97% in 48 h. The release rate of DAS was less than 30% in 48 h at pH 7.4 with GSH (2 uM). On the contrary, the amount of drug released at pH 7.4 and pH 6.0 without GSH were both less than 25% even after 144 h. Besides, the release amount of CP from CP-DDA NPs at corresponding conditions was also measured by HPLC, as shown in Fig. S6. The release rate of CP at pH 7.4 and pH 6.0 were 5.24% and 22.49%, respectively. The release rate of CP at pH 7.4+GSH and pH 6.0+GSH reached to 32.18% and 92.93%, respectively. The drug release behavior under different conditions indicated that this ADDC-based drug self-delivery system could remain stable in circulation, while rapidly releasing DAS and CP in tumor cells in reducing substances.

3.6. *In vitro cytotoxicity*

In order to evaluate the cytotoxicity, DAS, CP, CP+DAS and CP-DDA NPs with different concentrations were treated with H22 and HepG2 cells for 24 h. Different concentrations of DAS, CP, DAS+CP and CP-DDA NPs were co-incubated with H22 and HepG2 cells. After incubating for 24 h, cell viabilities were measured by MTT assay, and the results were shown in Fig. 2. DAS showed mild toxicity to H22 and HepG2 cells, since the cell survival rate was larger than 70% within the largest tested concentrations. In the contrast, CP, CP+DAS and CP-DDA NPs showed dose-dependent cytotoxicity. For H22 cells, the survival rate was 55.53% after incubated with free CP (16 ug/ml) for 24 h, and the cell viabilities of CP+DAS (47.78 + 16 ug/ml) treated H22 were 42.13% (24 h), while the corresponding survival rates of CP-DDA NPs (78.61 ug/ml) were 61.56%, respectively. For HepG2 cells, CP, CP+DAS and CP-DDA show similar cytotoxicity to H22. It should be noted that the cytotoxicity of CP-DDA NPs on HepG2 and H22 is less than that of CP and CP+DAS. This can be due to the slow release of the drug resulted from the fact that CP-DDA NPs need to be degraded under reducing conditions after being taken up by tumor cells.

3.7. *Cell apoptosis measurement*

In order to further verify the efficacy of CP-DDA NPs, H22 and HepG2 cells were co-incubated with all these samples. Cell apoptosis were detected via flow cytometry after 24 h (Fig. 3). DAS only displayed mild cytotoxicity at detected concentration, as the apoptosis rate (Q2+Q3) was only 11.83% (H22) and 9.78% (HepG2). Besides, the apoptosis rate of CP-DDA NPs (Q2+Q3) was 32.7% (H22) and 37.19% (HepG2), respectively, slightly higher than CP (23.26%, 22.65%) and lower than CP+DAS (44.8%, 53.52%), which was consistent with the result of MTT.

3.8. *Evaluation of the healing and migration abilities of tumor cells In vitro*

DAS is a Src inhibitor, which is reported to suppress the proliferation and metastasis of various cancer cells. Therefore, the ability of each sample that restrain the HepG2 cells

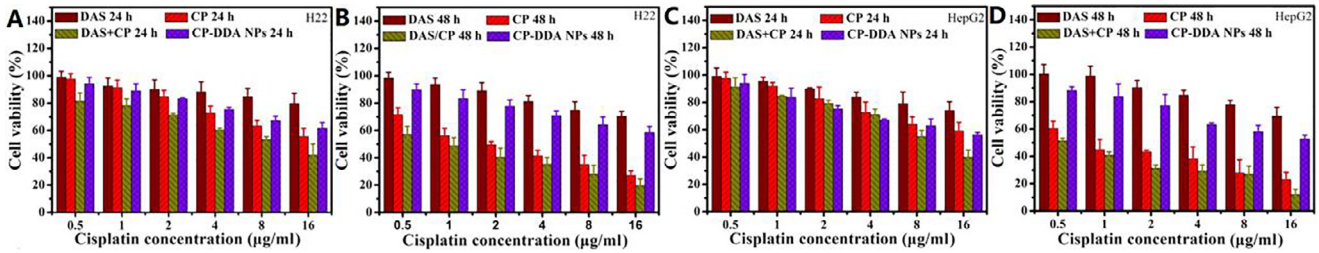

Fig. 2 – *In vitro* cytotoxicity of DAS, CP, DAS+CP and CP-DDA NPs against H22 cells for 24 h (A) and 48 h (B); *In vitro* cytotoxicity of DAS, CP, DAS+CP and CP-DDA NPs against HepG2 cells for 24 h (C) and 48 h (D).

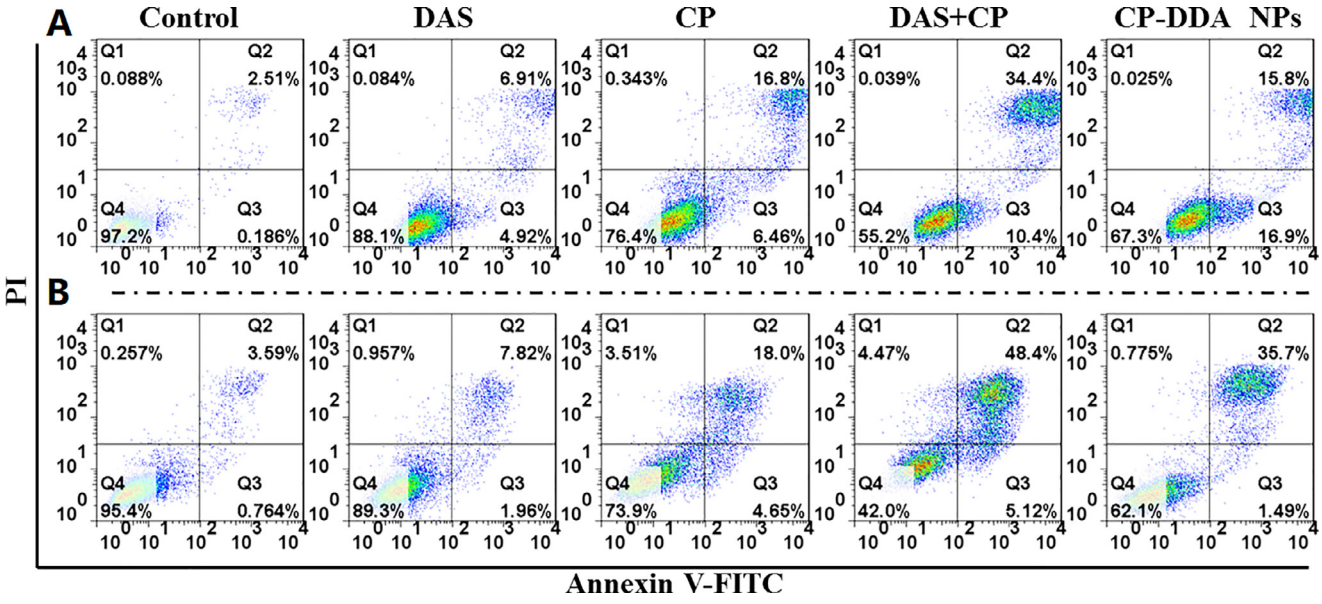

Fig. 3 – *In vitro* cell apoptosis evaluation of DAS, CP, DAS+CP and CP-DDA NPs against H22 cells (A) and HepG2 cells (B) for 24 h.

proliferation was verified by a plate scratch experiment, as shown in Fig. 4A. It was found that compared with control group, DAS, CP, CP+DAS and CP-DDA NPs significantly inhibited the migration and proliferation of HepG2 cells. The healing rate of the control group was 50% (Fig. 4B) after 48 h, while the healing rate of DAS was reduced to 0. It is worth noting that CP (−23.07%), CP+DAS (−25%) and CP-DDA NPs (−20%) not only completely inhibited the healing but also increased the scratch width of HepG2. This result indicated that this ADDC-based CP-DDA NPs could combine the cytotoxicity of CP and the ability of DAS to inhibit tumor cell migration and proliferation, thereby exerting a synergistic therapeutic effect.

Transwell experiment further verified the inhibition of each drug formulation on cell migration. Compared with the control, the cell migration ability after treatment with different drugs were significantly reduced (Fig. 4C and 4D). In the control group, large number of cells passed through the transwell and adhered to the membrane to grow, and the cell morphology was spindle-shaped. After CP treatment, a certain proportion of cells still passed through the transwell. In contrast, after treatment with DAS, CP+DAS and CP-DDA NPs, only a few cells were able to pass through the transwell. This result once again proves that the combination of DAS and CP can effectively inhibit the migration of tumor cells.

3.9. *Preparation and growth inhibition study of HepG2 MCS*

In order to verify *in vitro* anti-tumor activity of the prepared CP-DDA NPs, HepG2 MCS was incubated with the above-mentioned various drug formulations for 3 days, and then the inhibitory effect of each drug on MCS was observed. Fig. 5 showed the representative pictures of MCS during the treatment. For control group (MCS with fresh medium), peripheric cells of MCS proliferated continually from 0 to 3 d, leading to a significant growth in size and the final average diameter reached to 247.46 um. Besides, DAS only displayed a certain inhibitory effect on the growth of MCS. Thus, the diameter of MCS had only a slightly growth after 3 d (172.81 um). On the contrary, CP, CP+DAS and CP-DDA NPs showed a remarkable inhibitory effect on MCS. During the diameter and volume of MCS continued to shrink, and the average diameter of each group was 75.4 um (CP), 67.7 um (DAS+CP) and 90.4 um (CP-DDA NPs) at the end of the experiment, respectively. For CP-DDA NPs, the outer layer cells

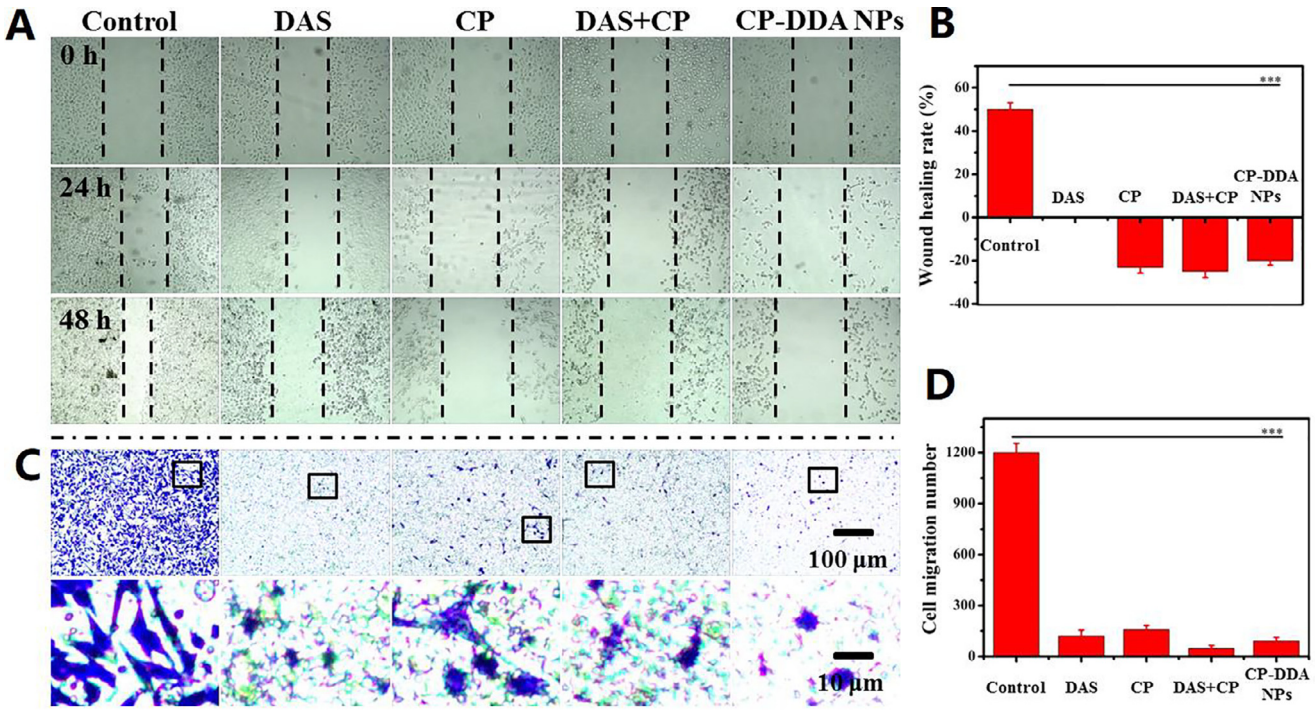

Fig. 4 – HepG2 cell wound healing (A) and healing rate (B); transwell migration experiments (C) and migration number (D).

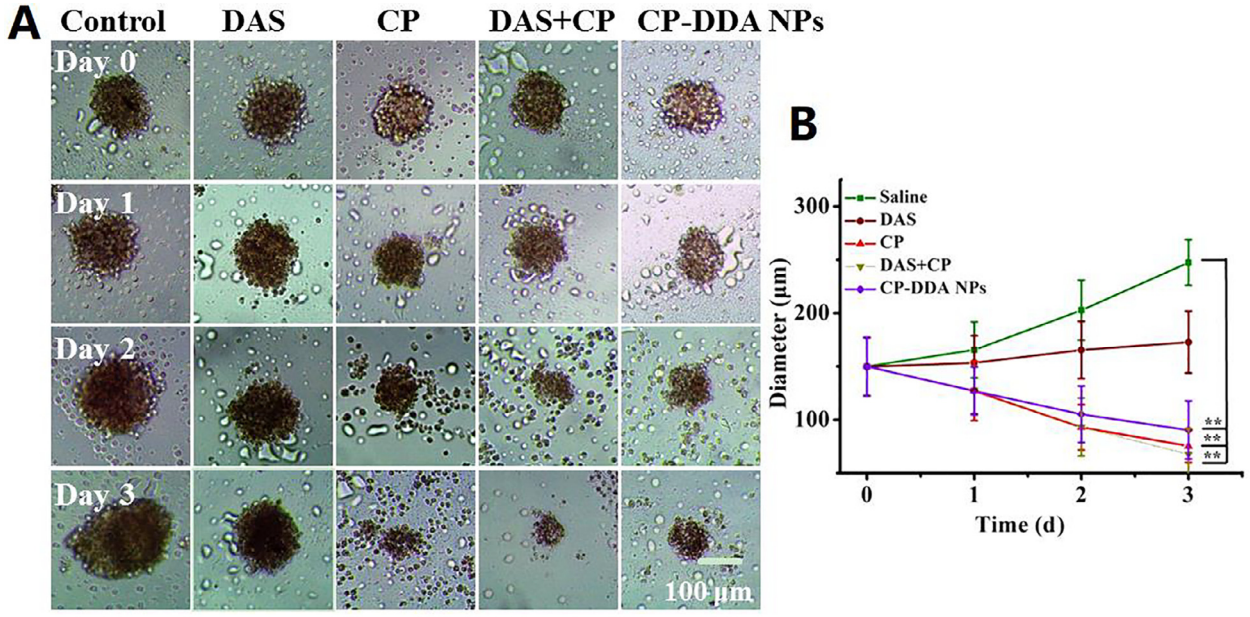

Fig. 5 – Representative images of HepG2 MCS in growth inhibition assay (A) and diameter change carve of MCS (B).

of MCS died and fell off, and the 3D structure of MCS was destroyed at the end of the treatment.

3.10. *In vivo antitumor experiment and immunohistochemistry*

In vivo antitumor effect of DAS, CP, DAS+CP and CP-DDA NPs was then investigated in subcutaneous H22 tumor-bearing mice. The average tumor volume of mice in all groups was shown in Fig. 6B. For saline-treated mice, the tumor volume was 649.11 mm^3 at Day 7, while the tumor volume of DAS-treated mice was 454.18 mm^3. Compared with CP-DDA NPs, CP and DAS+CP show higher tumor suppressing ability, as the tumor volume at Day 7 was 167.44 mm^3 (CP), 114.76 mm^3 (DAS+CP) and 211.79 mm^3 (CP-DDA NPs), respectively. CP and DAS+CP can effectively inhibit tumor growth in the initial of the study. However, the mice in the CP and DAS+CP-treated groups began to die on the 7th and 4th d, respectively, which

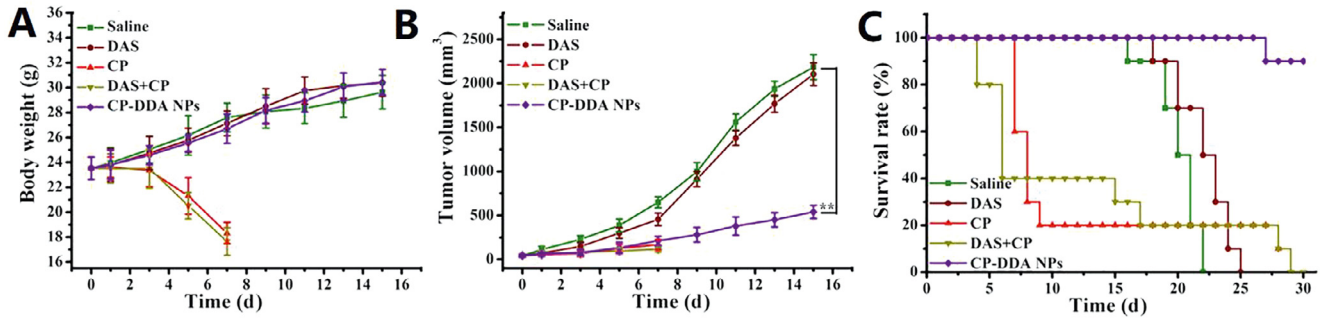

Fig. 6 – *In vivo* antitumor assay: Tumor growth curves of mice (A), body weight change of mice (B), and survival rate change (C) in HepG2 tumor-bearing mice after intravenous injection of saline, DAS, CP, DAS+CP and CP-DDA NPs.

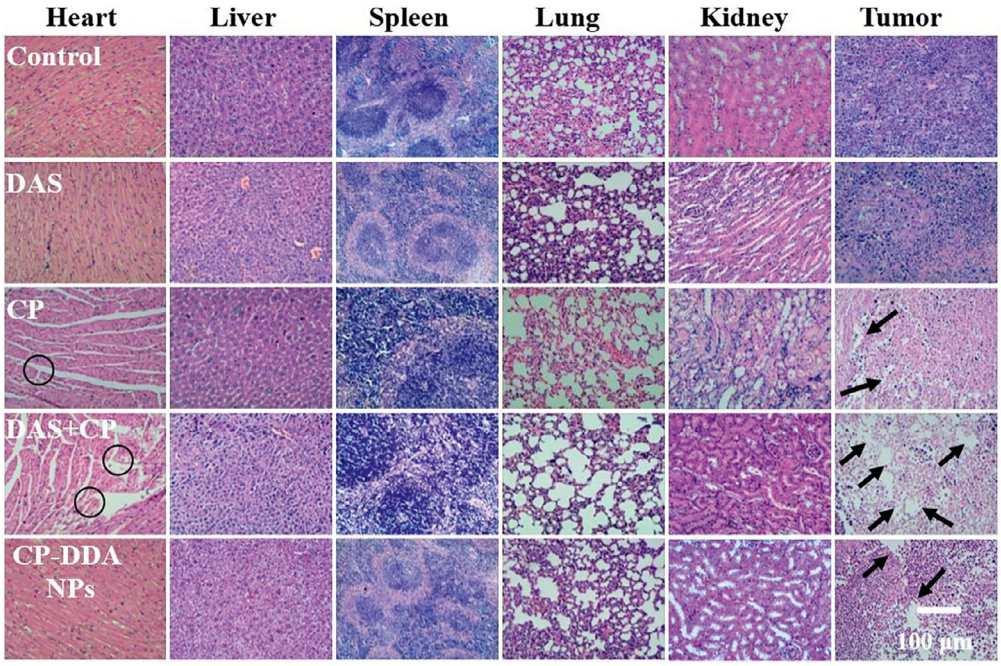

Fig. 7 – Histopathological analysis of sections stained with H&E.

could be caused by the strong toxicity of free CP (Fig. 6C). On the 15th day after administration, the survival rate of CP and DAS+CP-treated mice reduced to 20% and 30%, respectively, while the survival rate of CP-DDA NPs-treated mice was 100%. In addition, CP, DAS, and DAS+CP-treated mice all died within 30 d, while the survival rate of CP-DDA NPs-treated mice was 90%. This result shows that CP-DDA NPs can effectively reduce the toxicity of the two drugs, which is also one of the most important advantages of nanoforms. The tumor volume of saline, DAS and CP-DDA NPs-treated mice continued to be recorded for 15 d At the end, the tumor volume of saline-treated mice was 2183.82 mm^3, which was twenty times the initial volume. CP-DDA NPs showed the superiority antitumor activity, as the tumor volume was 539.11 mm^3, which was five times as the initial. In addition, the survival rate of mice in the CP-DDA NPs group was 90% on Day 30, which was much better than the other groups. The anti-tumor data showed that the carrier-free drug-self delivery system had excellent anti-tumor effects, while significantly reducing the toxicity of CP.

To further study the biosafety and biocompatibility of CP-DDA NPs, the main organs and tumors of mice in all groups were removed on Day 5 for histological examination (Fig. 7). Obviously, there was no significant tissue damage in DAS and CP-DDA NPs-treated mice, while CP and DAS+CP showed severe cardiac toxicity (the area marked by the black circle). The tumor treated with saline exhibited scarcely apoptotic region with a large amount of proliferating activity cells (Blue nucleus), while free DAS-treated tumors displayed a few apoptotic areas surrounded by live tumor cells. On the contrary, large apoptotic or necrotic region could be found in the tumor of CP, CP+DAS and CP-DDA NPs-treated mice (black arrows indicated to the apoptotic or necrotic area). These results further demonstrated that the carrier-free drug self-delivery system designed based on amphiphilic drug-drug conjugates (ADDC) significantly reduced the toxicity

and side effects of CP while retaining the synergistic effects of drugs.

4. Conclusion

Based on CP and DAS, an amphiphilic drug-drug conjugate was successfully prepared through a simple reaction, and further self-assembled to form a carrier-free drug self-delivery system (CP-DDA NPS). CP-DDA NPs have appropriate physiological stability, which can effectively avoid the toxicity of free drugs to normal tissues. In addition, CP-DDA NPs can be degraded with high concentrations of GSH, which can achieve the precise release of DAS and Pt(II) in tumor cells. *In vitro* cell experiments show that DAS is less toxic to tumor cells, but it can effectively inhibit the proliferation and migration of tumor cells. The combination with CP can enhance the cytotoxicity of CP. *In vivo* anti-tumor experiments show that CP-DDA NPs can significantly inhibit the growth of tumors, and reduce the toxic and side effects of CP. The survival rate of mice within 30 d reaches 90%, which is much higher than that of CP or CP+DAS-treated mice. Thus, the nanoparticles based on CP and DAS conjugates can effectively avoid the toxic and side effects of free drugs, enhance the anti-tumor activity of CP, and have potential applications.

Conflicts of interest

The authors report no conflicts of interest. The authors alone are responsible for the content and writing of this article.

Acknowledgments

This work was supported by the National Natural Science Foundation of China (No. 51803001 and 51503001), the Natural Science Foundation of Anhui Province (No. 2008085ME136 and 2008085QE210), the Research Foundation of Education Department of Anhui Province of China (No. KJ2018ZD003, KJ2018A0006 and KJ2019A0015), and the Academic and Technology Introduction Project of Anhui University (AU02303203) grant.

Supplementary materials

Supplementary material associated with this article can be found, in the online version, at doi:10.1016/j.ajps.2021.08.001.

REFERENCES

[1] Li J, Li B, Sun L, Duan B, Huang S, Yuan Y, et al. Self-delivery nanoparticles of an amphiphilic irinotecan-enediyne conjugate for cancer combination chemotherapy. J Mater Chem B 2019;7(1):103–11.
[2] Huttunen KM, Raunio H, Rautio J. Prodrugs-from serendipity to rational design. Pharmacol Rev 2011;63(3):750–71.
[3] Qin S, Zhang A, Cheng S, Rong L, Zhang X. Drug self-delivery systems for cancer therapy. Biomaterials 2017;112:234–47.
[4] Zhang Y, Yin R, Wu G, Yu M, Liu J, Wang X, et al. Self-assembling nanoparticles of dually hydrophobic prodrugs constructed from camptothecin analogue for cancer therapy. Eur J Med Chem 2020;200:112365.
[5] Zhou Q, Shao S, Wang J, Xu C, Xiang J, Piao Y, et al. Enzyme-activatable polymer-drug conjugate augments tumour penetration and treatment efficacy. Nat Nanotechnol 2019;14(8):799–809.
[6] Lv S, Wu Y, Cai K, He H, Li Y, Lan M, et al. High drug loading and sub-quantitative loading efficiency of polymeric micelles driven by donor-receptor coordination interactions. J Am Chem Soc 2018;140(4):1235–8.
[7] Song J, Lin L, Yang Z, Zhu R, Zhou Z, Li Z, et al. Self-assembled responsive bilayered vesicles with adjustable oxidative stress for enhanced cancer imaging and therapy. J Am Chem Soc 2019;141(20):8158–70.
[8] Gao C, Bhattarai P, Chen M, Zhang N, Hameed S, Yue X, et al. Amphiphilic drug conjugates as nanomedicines for combined cancer therapy. Bioconjugate Chem 2018;29(12):3967–81.
[9] Wang Y, Yang P, Zhao X, Gao D, Sun N, Tian Z, et al. Multifunctional cargo-free nanomedicine for cancer therapy. Int J Mol Sci 2018;19(10):2963–83.
[10] Ma P, Chen J, Bi X, Li Z, Gao X, Li H, et al. Overcoming multidrug resistance through the GLUT1-mediated and enzyme-triggered mitochondrial targeting conjugate with redox sensitive paclitaxel release. ACS Appl Mater Inter 2018;10(15):12351–63.
[11] Dong S, He J, Sun Y, Li D, Li L, Zhang M, et al. Efficient click synthesis of a protonized and reduction-sensitive amphiphilic small-molecule prodrug containing camptothecin and gemcitabine for a drug self-delivery system. Mol Pharmaceut 2019;16(9):3770–9.
[12] Wang J, Tang J, Fan M, Van K, Shen Y, Jin E, et al. Prodrugs forming high drug loading multifunctional nanocapsules for intracellular cancer drug delivery. J Am Chem Soc 2010;132(12):4259–65.
[13] Fan L, Zhang B, Xu A, Shen Z, Guo Y, Zhao R, et al. Carrier-free, pure nanodrug formed by the self-assembly of an anticancer drug for cancer immune therapy. Mol Pharmaceut 2018;15(6):2466–78.
[14] Zhang X, Zhang M, Wang M, Peng H, Hua Q, Ma L, et al. Facile fabrication of 10-hydroxycamptothecin-backboned amphiphilic polyprodrug with precisely tailored drug loading content for controlled release. Bioconjugate Chem 2018;29(7):2239–47.
[15] Cong Y, Xiao H, Xiong H, Wang Z, Ding J, Li C, et al. Dual drug backboned shattering polymeric theranostic nanomedicine for synergistic eradication of patient-derived lung cancer. Adv Mater 2018;30(11):1–11.
[16] Lu Y, Aimetti AA, Langer R, Gu Z. Bioresponsive materials. Nat Rev Mater 2016;1:16075.
[17] Hu Q, Sun W, Wang C, Gu Z. Recent advances of cocktail chemotherapy by combination drug delivery systems. Adv Drug Deliv Rev 2016;98:19–34.
[18] Wang Z, Chen J, Little N, Lu J. Self-assembling prodrug nanotherapeutics for synergistic tumor targeted drug delivery. Acta Biomater 2020;111:20–8.
[19] He W, Hu X, Jiang W, Liu R, Zhang D, Zhang J, et al. Rational design of a new self-codelivery system from redox-sensitive camptothecin–cytarabine conjugate assembly for effectively synergistic anticancer therapy. Adv Healthc Mater 2017;6(24):1–13.
[20] Xu S, Zhu X, Huang W, Zhou Y, Yan D. Supramolecular cisplatin-vorinos- tat nanodrug for overcoming drug

resistance in cancer synergistic therapy. J Control Release 2017;266:36–46.
[21] Liang X, Gao C, Cui L, Wang S, Wang J, Dai Z. Self-assembly of an amphiphilic janus camptothecin-floxuridine conjugate into liposome-like nanocapsules for more efficacious combination chemotherapy in cancer. Adv Mater 2017;29(40):1–9.
[22] Hou M, Li S, Xu Z, Li Z. A Reduction-responsive amphiphilic methotrexate-podophyllotoxin conjugate for targeted chemotherapy. Chem-Aslan J 2019;14(21):3840–4.
[23] Gao C, Bhattarai P, Chen M, Zhang N, Hameed S, Yue, et al. Amphiphilic drug conjugates as nanomedicines for combined cancer therapy. Bioconjugate Chem 2018;29(12):3967–81.
[24] Zhang J, Nie W, Chen R, Chelora J, Wan Y, Cui X, et al. Green mass production of pure nanodrugs via an ice-template-assisted strategy. Nano Lett 2019;19(2):658–65.
[25] Huang P, Wang D, Su Y, Huang W, Zhou Y, Cui D, et al. Combination of small molecule prodrug and nanodrug delivery: amphiphilic drug-drug conjugate for cancer therapy. J Am Chem Soc 2014;136(33):11748–56.
[26] Mayer EL, Krop IE. Advances in targeting Src in the treatment of breast cancer and other solid malignancies. Clin Cancer Res 2020;16(14):3526–32.
[27] Wang L, Guo B, Wang R, Jiang Y, Qin S, Liang S, Zhao Y, et al. Inhibition of cell growth and up-regulation of MAD2 in human oesophageal squamous cell carcinoma after treatment with the Src/Abl inhibitor dasatinib. Clin Sci 2012;122(1):13–24.
[28] Hughes VS, Siemann DW. Treatment with Src inhibitor Dasatinib results in elevated metastatic potential in the 4T1 murine mammary carcinoma model. Tumor Mic 2018;1(1):30–6.
[29] John A, Christopher L. Dasatinib: a potent SRC inhibitor in clinical development for the treatment of solid tumors. Cancer Treat Rev 2010;36(6):492–500.
[30] Irby RB, Yeatman TJ. Role of Src expression and activation in human cancer. Oncogene 2010;19(49):5636–42.
[31] Antonio G, Ilaria M, Nicola S, Angelo V, Vito L. Dasatinib: an anti-tumour agent via Src inhibition. Curr Drug Targets 2011;12(4):563–78.
[32] Liang W, Kujawski M, Wu J, Lu J, Herrmann A, Loera S, et al. Antitumor activity of targeting Src kinases in endothelial and myeloid cell compartments of the tumor microenvironment. Clin Cancer Res 2010;16(3):924–35.
[33] Zhang X, Zang X, Qiao M, Zhao X, Hu H, Chen D. Targeted delivery of Dasatinib to deplete tumor-associated macrophages by mannosylated mixed micelles for tumor immunotherapy. ACS Biomater Sci Eng 2010;6(10):5675–84.
[34] Sun J, Liu Y, Chen Y, Zhao W, Zhai Q, Rathod S, et al. Doxorubicin delivered by a redox-responsive dasatinib-containing polymeric prodrug carrier for combination therapy. J. Control Release 2017;258:43–55.
[35] Ma L, Wei J, Su G, Lin J. Dasatinib can enhance paclitaxel and gemcitabine inhibitory activity in human pancreatic cancer cells. Cancer Biol Ther 2019;20(6):855–65.
[36] Chen J, Lan T, Zhang W, Dong L, Kang N, Fu M, et al. Dasatinib enhances cisplatin sensitivity in human esophageal squamous cell carcinoma (ESCC) cells via suppression of PI3K/AKT and Stat3 pathways. Arch Biochem Biophys 2015;575:38–45.
[37] Shen W, Luan J, Cao L, Sun J, Yu L, Ding J. Thermogelling polymer-platinum(IV) conjugates for long-term delivery of cisplatin. Biomacromolecules 2015;16(1):105–15.
[38] Mangrum JB, Farrell NP. Excursions in polynuclear platinum DNA binding. Chem Commun 2010;46(36):6640–50.
[39] He L, Sun M, Cheng X, Xu Y, Lv X, Wang X, et al. pH/Redox dual-sensitive platinum (IV)-based micelles with greatly enhanced antitumor effect for combination chemotherapy. J Colloid Interf Sci 2019;541:30–41.
[40] Kim EMH, Mueller K, Gartner E, Boerner J. Dasatinib is synergistic with cetuximab and cisplatin in triple-negative breast cancer cells. J Surg Res 2013;185:231–9.
[41] Ceppi P, Papotti M, Monica V, Lo M. Effects of Src kinase inhibition induced by dasatinib in non–small cell lung cancer cell lines treated with cisplatin. Mol. Cancer Ther. 2009;8:3066–74.
[42] Păunescu E, Clavel CM, Nowak-Sliwinska P, Griffioen AW, Dyson PJ. Improved angiostatic activity of Dasatinib by modulation with hydrophobic chains. ACS Med Chem Lett 2015;6(3):313–17.
[43] Lei M, Sha S, Wang X, Wang J, Du X, Miao H, et al. Co-delivery of paclitaxel and gemcitabine via a self-assembling nanoparticle for targeted treatment of breast cancer. RSC Adv 2019;9(10):5512–20.
[44] Kobayashi H, Watanabe R, Choyke PL. Improving conventional enhanced permeability and retention (EPR) effects; what is the appropriate target? Theranostics 2013;4(1):81–9.